Matrix Biology Plus 28 (2025) 100186

Contents lists available at ScienceDirect

Matrix Biology Plus

journal homepage: www.sciencedirect.com/journal/matrix-biology-plus

Generation of a conditional *Adamts6* mouse allele reveals roles in lung maturation in addition to cardiac and musculoskeletal development

Jessica M. Sirek [a,b], Elizabeth H. Rush [b,c], Aditi Darodkar [b], Suneel S. Apte [d], Timothy J. Mead [a,b,c,e,*]

[a] Department of Genetics and Genome Sciences, Case Western Reserve University, School of Medicine, Cleveland, OH 44106, United States
[b] Department of Pediatrics, Case Western Reserve University School of Medicine, Cleveland, OH 44106, United States
[c] Department of Biology, Case Western Reserve University School of Arts and Sciences, Cleveland, OH 44106, United States
[d] Department of Biomedical Engineering, Cleveland Clinic Research, Cleveland, OH 44195, United States
[e] Division of Pediatric Cardiology, University Hospitals Rainbow Babies and Children's Hospital, Cleveland, OH 44106, United States

ARTICLE INFO

Keywords:
ADAMTS protease
Metalloprotease
Extracellular matrix
Lung
Congenital heart defect
Musculoskeletal
Floxed

ABSTRACT

Prior analysis of mouse embryos homozygous for a point mutation (p.Ser149Arg) that abrogated secretion of the protease, ADAMTS6, showed that it is essential for cardiovascular and limb development. Because *Adamts6*$^{S149R/S149R}$ mice do not survive past birth, it is currently not feasible to investigate ADAMTS6 in specific cellular lineages postnatally. Therefore, we generated a conditional allele using CRISPR-Cas9-mediated genome editing to insert unidirectional loxP sites flanking the first coding exon in *Adamts6*, resulting in a frameshift mutation after loxP recombination. Mice homozygous for the unrecombined floxed allele (*Adamts6*$^{fl/fl}$) are viable, fertile, and without overt phenotype. *Adamts6*$^{del/del}$ embryos, generated upon constitutive recombination induced by a *CMV*-Cre transgene, also do not survive past birth and have identical defects in the heart and limbs as *Adamts6*$^{S149R/S149R}$ embryos, demonstrating efficient transgene recombination. In addition to previous defects in cardiovascular and limb development, *Adamts6*$^{del/del}$ embryos have reduced airway branching, thereby identifying a role for ADAMTS6 in lung maturation. This newly generated *Adamts6*^{fl} allele makes feasible analysis of ADAMTS6 secreted by cells of different lineages and during specified temporal windows during developmental processes as well as in disease models.

Introduction

A disintegrin-like and metalloprotease with thrombospondin type 1 motif (ADAMTS) genes encode secreted proteases that modify extracellular matrix (ECM) and cell-surface proteins, with numerous essential roles in adult tissue homeostasis and diverse disease processes [1]. ADAMTS6 and ADAMTS10 form a homologous pair in the family with each protease having distinct roles in development and postnatal biology [2,3]. For example, non-synonymous variants in *ADAMTS6* are linked to altered cardiac ventricular conduction, specifically a prolonged QRS interval, while *ADAMTS10* variants cause Weill-Marchesani syndrome, a connective tissue disorder characterized by short stature, joint stiffness, heart defects, and ocular lens dislocation [4,5]. In addition, ADAMTS6 has been linked to numerous cancers in many different organ systems such as breast, lung, colorectal, colon, and gastric with a pro- or anti-tumor association based upon the cancer type [6–10]. Recently, *ADAMTS6* mutations have been reported in a new human connective tissue disease, designated Connective tissue, Heart defect, thoracic Aortic aneurysm and Neuro developmental Syndrome (CHANS) [11].

To date, insights on ADAMTS6 function have been obtained using mice homozygous for point mutations generated using N-ethyl-N-nitrosourea (ENU) mutagenesis [12]. Of these mutants, we previously characterized one with a serine-to-arginine substitution at position 149 (p.Ser149Arg) [4]. The affected serine residue was conserved across multiple species and the substitution prevented secretion of the variant protein, essentially comprising a gene knockout [4]. *Adamts6* mRNA is expressed in various murine tissues, including cardiac tissues such as the myocardium, outflow tract, and heart valves, as well as musculoskeletal tissues including cartilage, tendons, and skeletal muscle [2,4]. Analysis of the mice also provided phenotype correlates with CHANS [11]. Previous research has identified ECM microfibril components, including

* Corresponding author at: Case Western Reserve University, School of Medicine (WRB4529), Cleveland, OH 44106, United States.
E-mail address: Timothy.Mead@case.edu (T.J. Mead).

https://doi.org/10.1016/j.mbplus.2025.100186
Received 24 July 2025; Received in revised form 23 October 2025; Accepted 17 November 2025
Available online 19 November 2025

fibrillin-1, fibrillin-2, fibronectin, and LTBP-1, as well as a cell-surface proteoglycan, syndecan-4, as ADAMTS6 substrates [2,13]. However, the full spectrum of substrates and cell-type specific roles is unknown.

Adamts6$^{S149R/S149R}$ mice exhibit a spectrum of congenital heart defects, including double outlet right ventricle, persistent truncus arteriosus, atrial and ventricular septation defects, and ventricular hypertrophy [4,12]. Although ADAMTS6 is recognized for its role in cardiovascular development, embryonic death of the mutants has precluded analysis of a role in cardiac function after birth. *Adamts6*$^{S149R/S149R}$ mice also have severe skeletal abnormalities affecting both the appendicular and axial skeleton, including clubfoot-like deformities, shortened and curved limb bones, delayed endochondral ossification, disorganized growth plates, and disrupted chondrogenic markers and it has emerged as a gene of significance in knee osteoarthritis through analysis showing that loss of function and mis-sense variants are protective against disease [1,14]. ADAMTS6 plays a key role in microfibril turnover, as its loss or inactivation in mice leads to excessive microfibril accumulation, whereas its overexpression in vitro prevented their formation. In particular, genetic rescue of limb and axial skeletal defects in *Adamts6*-deficient mice through *Fbn2* haploinsufficiency, but not through alteration of *Fbn1*, underscored a potentially specific role in regulating fibrillin-2 content in the context of skeletal development [2].

Given the obvious disease relevance, the embryonic lethality of the *Adamts6*$^{S149R/S149R}$ mutant has limited investigation of biological roles and lineage specific functions of ADAMTS6. To elucidate the functions of ADAMTS6 in specific tissues, at various developmental stages, and in adult pathologies, we have generated a floxed allele (*Adamts6*^{fl}) for targeted conditional inactivation. Here we provide an initial characterization of the new allele and validation of its use for conditional *Adamts6* inactivation.

Methods

Construction of the targeting vector

The *Adamts6* floxed allele was engineered using a targeting construct cloned into a high-copy plasmid backbone, pDonor[KI]-[*Adamts6* 5′-HA]:[*Adamts6* 3′-HA] (Vector ID: VB190823-1141hfw). The targeting vector contained unidirectional loxP sites flanking exon 1, enabling Cre-mediated excision. The 5′ and 3′ homology arms (HA) were derived by PCR from the *Adamts6* locus, with the 5′ HA of 1013 base pairs upstream of coding exon 1 and the 3′ HA of 983 base pairs downstream of coding exon 1, facilitating homologous recombination. A *Bam*HI site was positioned upstream and an *Xba*I site downstream of the loxP-flanked region for construct linearization. The vector backbone included an ampicillin-resistance gene for bacterial selection. The vector underwent restriction mapping and sequencing of the 5′ and 3′ ends and the loxP-flanked region, to confirm integrity of the insertion cassette and correct placement of loxP sites and HAs. To validate CRISPR-Cas9 targeting efficiency prior to *in vivo* application, guide RNA activity was evaluated using the Guide-it Complete sgRNA Screening System (632638, Takara), ensuring optimal sgRNA selection for precise loxP site insertion. The 5′ gRNAs AAATTGTTATGCTTCGATAT and CTATTGACTCTCTAGCTCAT and 3′ gRNAs CTTGGGAATATTTAGTCAGA and AAAACTCTGAGTATTTAGTT were used.

Generation of mice carrying the floxed Adamts6 allele

The targeting construct was linearized using restriction endonucleases *Bam*HI and *Xba*I prior to electroporation into embryonic stem (ES) cells of C57BL/6/SJL F1 hybrid DNA origin at the Case Western Reserve University Transgenic and Targeting Facility. Targeted ES cell clones were screened by PCR and sequencing to confirm integration of the loxP sites flanking exon 1 and the integrity of the 5′ and 3′ HAs. Correctly targeted ES cells were microinjected into Balb/c blastocysts. Resulting chimeras with a high percentage of black coat color were mated to wild type C57BL/6 mice to generate F1 hemizygous progeny. Tail DNA from pups with black coat color was used for genotyping by PCR (Supplementary Table 1).

The floxed allele (designated as *Adamts6*^{fl}) is maintained in the C57BL/6 strain and mice starting from the 5th generation of intercrossing were used. For germline deletion to test the efficiency of Cre-mediated excision in the floxed allele, *Adamts6*$^{fl/+}$ mice were crossed with *CMV*-Cre (Jackson Laboratory, 006054) mice to generate female *Adamts6*$^{fl/+}$;*CMV*-Cre offspring, which were then bred to *Adamts6*$^{fl/fl}$ male mice to obtain *Adamts6*$^{fl/fl}$;*CMV*-Cre embryos, referred to hereafter as *Adamts6*$^{del/del}$.

The mouse lines used in this study, including *Adamts6*$^{S149R/S149R}$ (originally designated *Adamts6*^{b2b2029Clo}; RRID:MGI:5487397), *CMV*-Cre (006054, Jackson Laboratory), *Tagln*Cre (017491, Jackson Laboratory) and *Gt(ROSA)26Sor*$^{tm4(ACTB-tdTomato,-EGFP)Luo}$/J designated further here as ROSA$^{mT/mG}$ (007576, Jackson Laboratory) were previously described and maintained on the C57BL/6J background. *Adamts6*$^{fl/+}$ mice were crossed with *Tagln*Cre mice and the ensuing *Adamts6*$^{fl/+}$;*Tagln*Cre offspring were bred with *Adamts6*$^{fl/fl}$ mice to obtain *Adamts6*$^{fl/fl}$;*Tagln*Cre mice. *Adamts6*$^{fl/+}$ mice were crossed with ROSA$^{mT/mG}$ mice and the ensuing *Adamts6*$^{fl/+}$;ROSA$^{mT/mG}$ offspring were bred with *Adamts6*$^{fl/fl}$ mice to obtain *Adamts6*$^{fl/fl}$;ROSA$^{mT/mG}$ mice. These mice were bred with *Adamts6*$^{fl/+}$;*CMV*-Cre to obtain *Adamts6*$^{del/del}$;*CMV*-Cre;ROSA$^{mT/mG}$ embryos. All animal experiments were conducted in accordance with institutional and national guidelines and were approved by the Cleveland Clinic (IACUC protocol 00002450) and the Case Western Reserve University Institutional Animal Care and Use Committee (IACUC protocol 2022-0070).

RNA isolation and quantitative real-time PCR (RT-qPCR) from mouse tissue

Mouse embryonic day (E)18.5 hindlimb, skin, muscle, and lung were snap-frozen and stored at −80 °C until use. Following tissue homogenization in TRIzol (15596018, Invitrogen) total RNA was reverse transcribed with SuperScript III CellsDirect cDNA synthesis system (46–6321, Invitrogen). cDNA was generated from 1 μg RNA using a High-Capacity cDNA reverse transcription kit following the manufacturer's instructions (4368814, Applied Biosystems). Power SYBR Green Mastermix (4367659, Applied Biosystems) was used for RT-qPCR using an Applied Biosystems 7500 instrument. The experiments were performed with replicate biological samples and reproducibility was confirmed with technical replicates. *Gapdh* served as the housekeeping gene. The ΔΔCt method was applied to calculate relative mRNA expression levels of target genes using GraphPad Prism. Supplementary Table 1 provides the primer sequences.

Mouse embryonic fibroblasts (MEFs) were generated from E14.5 *Adamts6*$^{del/del}$ and wild type littermate embryos as previously described [15]. The medium was discarded, and cells were washed with PBS. RNA isolation, cDNA synthesis and RT-qPCR were done as above.

Skeletal preparations

Alizarin red–alcian blue skeletal staining was performed following an established protocol [2,16]. Briefly, skinned and eviscerated E18.5 embryos were fixed in 80 % ethanol for 24 h, followed by dehydration in 95 % ethanol for 24 h and then in acetone for 48 h. Specimens were stained using a solution containing 0.1 % alizarin red S, 0.3 % alcian blue, and 1 % glacial acetic acid in 95 % ethanol for 48 h. After staining, samples were cleared in 95 % ethanol for 1 h, and muscle tissue was carefully removed using forceps. The preparations were then progressively cleared in a series of glycerol/1 % KOH solutions with increasing glycerol concentrations (20–80 %) before final storage in 100 % glycerol. Images were captured using a Leica S9i dissecting microscope and camera. Crown-to-rump and individual bone length measurements were performed in a blinded manner using NIH Fiji software [17].

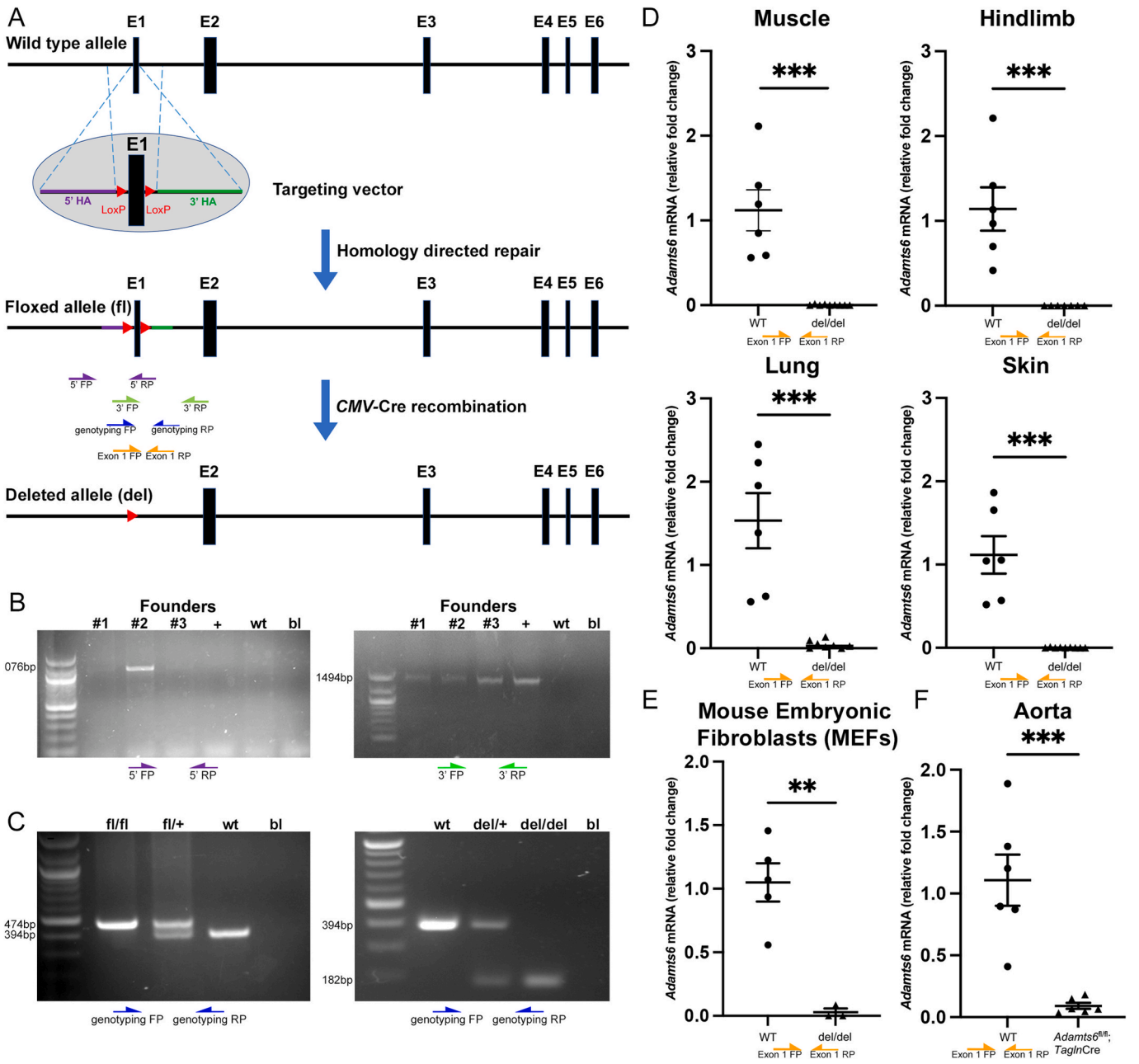

Fig. 1. Targeting strategy and confirmation of Cre-mediated homologous recombination and mRNA disruption. (A) A floxed *Adamts6* allele was generated using CRISPR-Cas9 and a targeting vector with unidirectional loxP sites flanking exon 1. **(B)** Three founders were genotyped and shown to have correct 5′ and 3′ recombination of the *Adamts6* gene with the targeting vector by PCR of genomic DNA. +, *Adamts6* targeting vector; bl, blank. **(C)** The genotyping strategy is illustrated using *Adamts6*^{fl} homozygous and heterozygous and wild type (wt) DNA (left-hand panel) and *Adamts6*^{del} homozygous and heterozygous and wt DNA (right-hand panel). **(D)** RT-qPCR of *Adamts6* RNA levels in wild type and *Adamts6*$^{del/del}$ muscle, hindlimb, lung and skin showing that *Adamts6* exon 1 is efficiently deleted by *CMV*-Cre. n = 6. **(E)** RT-qPCR analysis of wild type and *Adamts6*$^{del/del}$ mouse embryonic fibroblasts reveals efficient disruption of exon 1 in cells of *Adamts6*$^{del/del}$ embryos. n = 6. **(F)** RT-qPCR analysis of wild type and *Adamts6*$^{fl/fl}$;*Tagln*Cre aorta indicates substantial interruption of transcripts containing exon 1 of *Adamts6*. n ≥ 3. **p ≤ 0.01; ***p ≤ 0.001.

Histology and immunofluorescence microscopy

E18.5 tissue was fixed with 4 % paraformaldehyde (PFA) in PBS at 4 °C for 24 h. 7 μm sections were used for histochemistry (alcian blue, hematoxylin and eosin) or for indirect immunofluorescence. The primary antibodies (see Supplementary Table 2) were followed by secondary goat anti-mouse or goat anti-rabbit antibodies (A11004 or A11008, respectively, Invitrogen; 1:400) incubation. Prior to immunofluorescence, citrate antigen retrieval was performed by immersion of slides in citrate-EDTA buffer (10 mM/l citric acid, 2 mM/l EDTA, 0.05 % v/v Tween-20, pH 6.2) and microwaving for 4 intervals of 1.5 min at 50 % power in a microwave oven with 30 s intervals between heating cycles, was utilized. For alcian blue staining, sections were stained with 1 % alcian blue 8 GX (A3157, Sigma) in 3 % acetic acid (pH 2.5) for 10 min, rinsed in tap water, counter-stained in nuclear fast red (AAJ61010AU, ThermoFisher) for 1 min, and rinsed in tap water prior to dehydration and mounted, as previously described [18]. Images were obtained using a Leica DM4 B microscope with K3M and K3C cameras and Leica Application Suite X software. Histological sections were masked during data collection and quantified utilizing NIH Fiji software

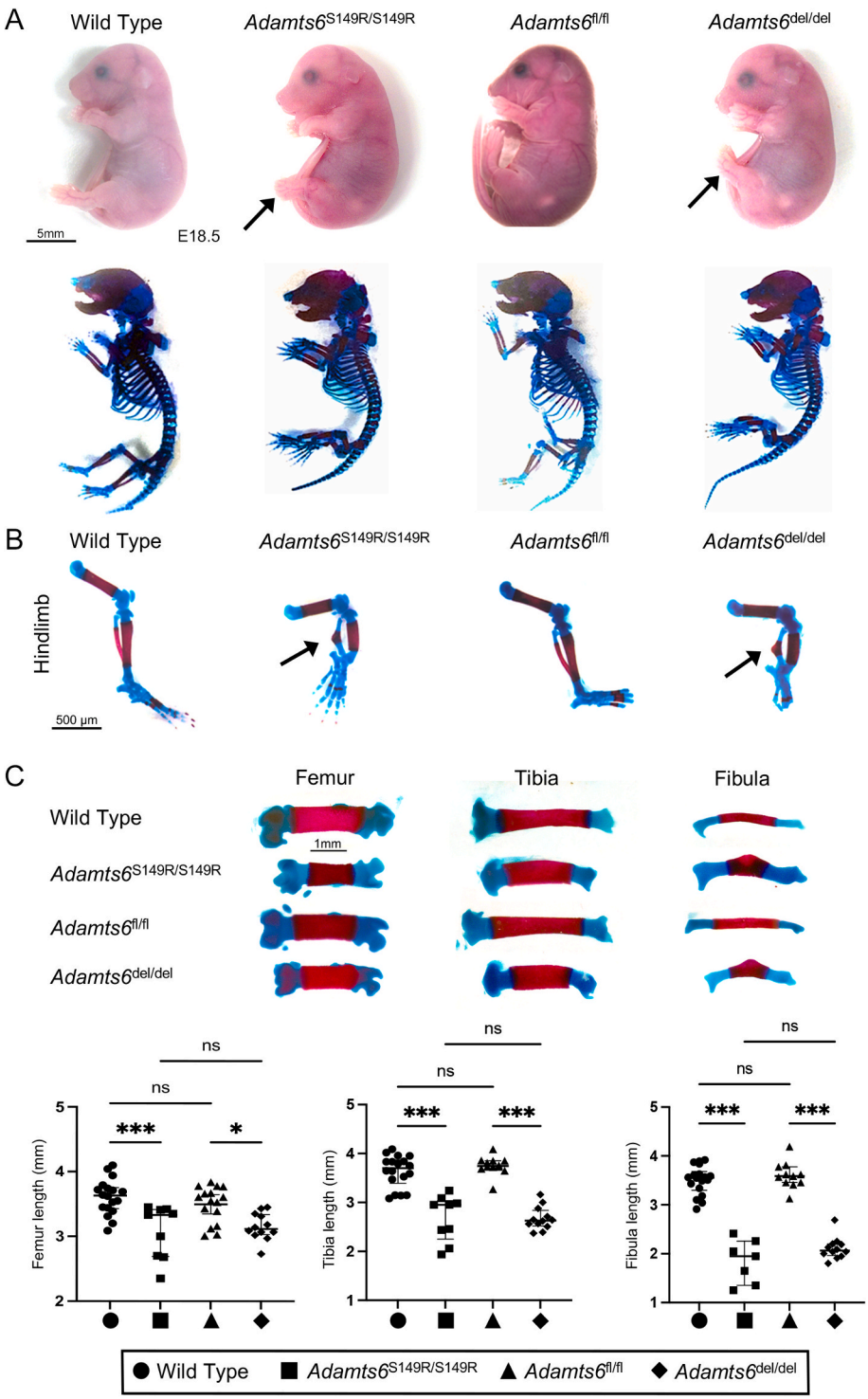

Fig. 2. *Adamts6* disruption results in skeletal abnormalities, including reduced long bone length and morphological malformations. (A) Gross anatomical assessment demonstrates that E18.5 *Adamts6*$^{del/del}$ embryos exhibit phenotypic abnormalities consistent with those observed in *Adamts6*$^{S149R/S149R}$ embryos, including a clubfoot-like malformation (black arrow). **(B)** Alizarin red and alcian blue-staining showed the skeletal basis of clubfoot-like deformities in both *Adamts6*$^{S149R/S149R}$ and Adamts6$^{del/del}$ hindlimbs compared to control. **(C)** Quantitative analysis reveals reduced length of the femur, tibia, and fibula in *Adamts6*-deficient mouse models as compared to control limbs. n ≥ 9. *p ≤ 0.05; ***p ≤ 0.001. (For interpretation of the references to colour in this figure legend, the reader is referred to the web version of this article.)

[17].

RNAscope in situ hybridization

RNAscope in situ hybridization was performed as previously described [19]. Briefly, wild type heart and lung slides were sectioned just prior to baking overnight at 60 °C. Slides were then placed in xylene and 100 % EtOH before air drying for 5 min. Hydrogen peroxide was used before slides were submerged in target retrieval for 15 min. The *Adamts6* probe (428301, Advanced Cell Diagnostics) was placed on

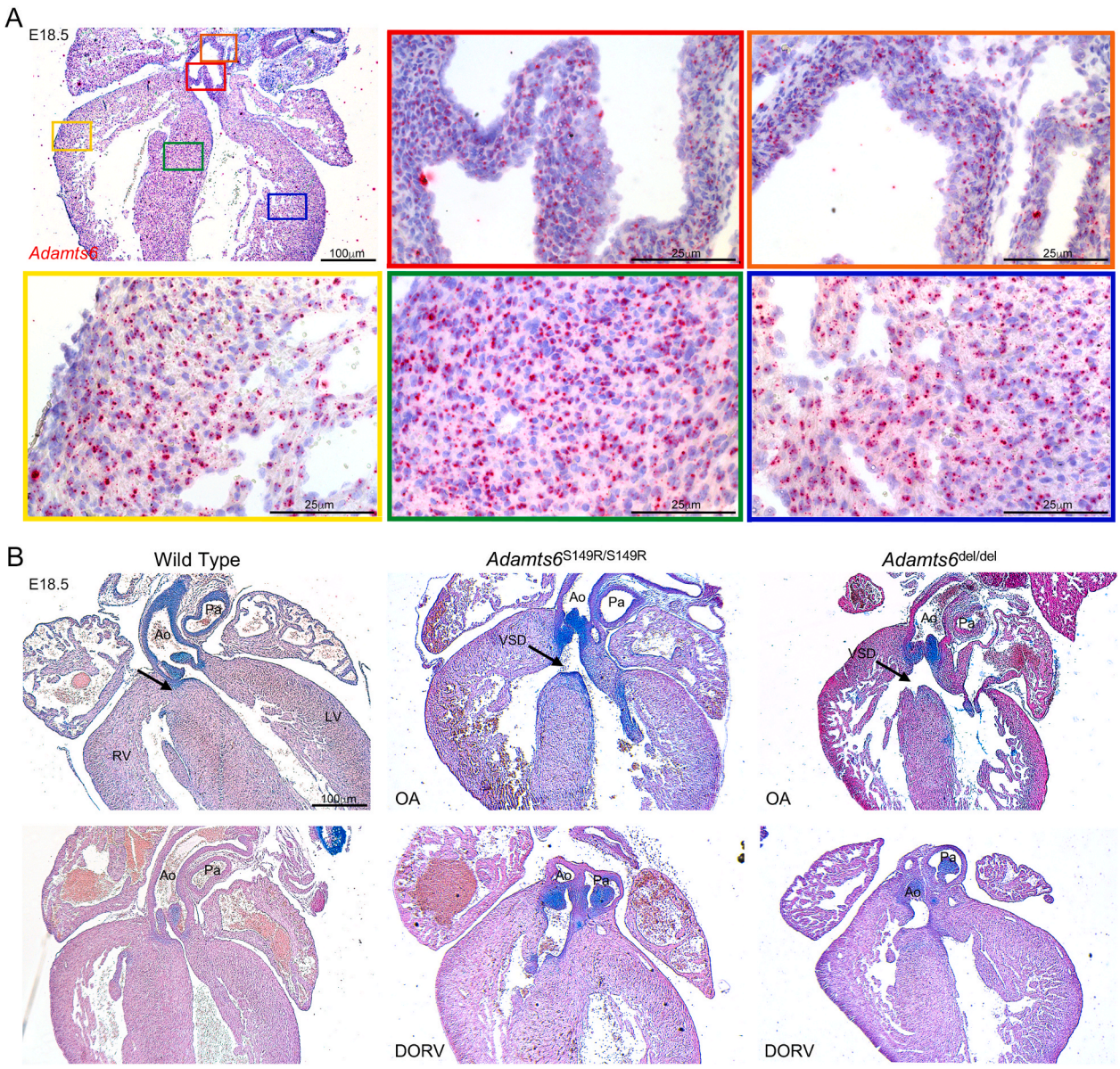

Fig. 3. *Adamts6*$^{del/del}$ embryos have congenital heart defects similar to those in *Adamts6*$^{S149R/S149R}$ mutants. (A) RNAscope in situ hybridization using a *Adamts6*-specific probe revealed region-specific expression within the E18.5 wild type heart, including the aortic valves, outflow tract (orange box), right ventricle (yellow box), intraventricular septum (green box), and left ventricle (blue box). **(B)** Alcian blue staining of E18.5 hearts from wild type embryos with the aorta (Ao), pulmonary artery (Pa), left ventricle (LV), right ventricle (RV) indicated and an arrow pointing to the location of the intraventricular septum. In contrast to wild type, *Adamts6*$^{S149R/S149R}$ and *Adamts6*$^{del/del}$ embryos showed ventricular septal defects (VSDs) and outflow tract defects such as overriding aorta (OA) and double outlet right ventricle (DORV). (For interpretation of the references to colour in this figure legend, the reader is referred to the web version of this article.)

slides for 2 hr at 40 °C before a series of amplification steps (322373, RNAscope RED detection Advanced Cell Diagnostics). Red working solution and 50 % hematoxylin (26030-10, Electron Microscopy Supplies) were used to visualize the RNA signal and washed with 0.02 % ammonia water until slides turned blue. Slides were dipped in xylene before being mounted in cytoseal (H-5000, VectaMount) and imaged the following day.

Quantitation of airway space

Paraffin sections from E18.5 lungs of wild type, *Adamts6*$^{fl/fl}$, *Adamts6*$^{S149R/S149R}$ and *Adamts6*$^{del/del}$ were analyzed. Images were taken from 6 representative embryos of each genotype. Images were obtained using a Leica DM4 B microscope with K3M and K3C cameras and Leica Application Suite X software. The sections were masked during data collection and were measured by three independent reviewers blinded to the genotype using ImageJ [20].

Immunocytochemistry

Wild type and *Adamts6*$^{del/del}$ MEFs were plated in an 8 well chamber slide (53106-306, Corning) at 12,000 cells per well. After 4 days, culture medium was discarded, and cells were washed with PBS, then fixed with 4 % paraformaldehyde for a 20 min incubation and blocked with 5 % normal goat serum in PBS for 1 h. Primary antibodies to fibrillin-1 and fibronectin (see Supplementary Table 2) diluted in 5 % normal goat serum in PBS were placed on cells overnight at 4 °C, cells were washed with PBS and secondary antibody was applied (A11041, ThermoFisher; 1:400; A11008, Life Technologies; 1:400) for 1 h. Cells were washed with PBS, and DAPI was added as a nuclear stain (D8417, Sigma;

1:10,000). Cells were cover slipped with ProLong Gold (9071S, Cell Signal Technology) and imaged with a Leica DM4 B microscope with K3M and K3C cameras and Leica Application Suite X software.

Statistics

ANOVA and unpaired *t* test were used to obtain p values. Asterisks indicate differences with statistical significance as follows: *p ≤ 0.05; **p ≤ 0.01; ***p ≤ 0.001. Grubb's outlier test was used on all data points to identify outliers.

Results

Transcriptional analysis of Adamts6 in Adamts6$^{del/del}$ embryos

The targeting construct was designed for excision of the first coding exon 1 by Cre-recombinase, resulting in a frameshift mutation (Fig. 1A). Among the 113 mice screened, 3 founders were identified with successful recombination at both loxP sites (Fig. 1B). These founders were subsequently bred to wild type C57BL/6 mice to ensure germline transmission and founder 2 was chosen to establish a transgenic line and correct targeting and genotyping were reconfirmed (Fig. 1C). To evaluate RNA expression in the *Adamts6*$^{del/del}$ mouse, RT-qPCR was performed on cDNA derived from muscle, hindlimb, lung, skin and MEFs of both *Adamts6*$^{del/del}$ and wild type mice (Fig. 1D and E) (primers in Supplementary Table 1). This demonstrated absence of exon 1 containing transcripts of *Adamts6*, confirming efficient deletion (Fig. 1D and E; Supplementary Fig. 1B, F). PCR spanning introns 1–4 showed a 96-base pair reduction in product size in *Adamts6*$^{del/del}$ samples compared to wild type, consistent with Cre-mediated excision of exon 1 (Supplementary Fig. 1C, F). In contrast, amplification of exons 4–6 produced products of the expected size in both genotypes, indicating that downstream transcription may remain intact (Supplementary Fig. 1D, F). *Gapdh* amplification was consistent across all samples, confirming the integrity of the cDNA and PCR reactions and was quantified to normalize intensity (Supplementary Fig. 1E). Analysis of *Adamts6*$^{fl/fl}$;*CMV*-Cre;Rosa$^{mT/mG}$ showed tdTomato fluorescence was replaced by membrane-localized EGFP (mG), providing visual confirmation of recombination efficiency in the *Adamts6*$^{fl/fl}$;*CMV*-Cre embryos (Supplementary Fig. 2). *Adamts6*$^{del/del}$ embryos were collected at the expected Mendelian ratio at the end of the embryonic period (E18.5). In a survival study, 9 litters totaling 70 pups were collected at birth with all (19/19) stillborn pups genotyped identified as *Adamts6*$^{del/del}$. Wild type and *Adamts6*$^{del/+}$ mice were at the expected Mendelian ratios.

Having validated that the *Adamts6*$^{fl/fl}$ allele permits conditional gene inactivation, *Adamts6*$^{fl/fl}$;*Tagln*Cre mice were generated to achieve smooth muscle-specific deletion of *Adamts6*. As assessed by RT-qPCR, *Adamts6* expression was significantly reduced in the aorta of *Adamts6*$^{fl/fl}$;*Tagln*Cre mice as compared to control (Fig. 1F).

Severe skeletal malformations in Adamts6$^{del/del}$ embryos replicated chondrodysplasia seen in Adamts6$^{S149R/S149R}$ mutant embryos

Adamts6$^{S149R/S149R}$ and *Adamts6*$^{del/del}$ embryos shared gross anatomical differences compared to wild type and *Adamts6*$^{fl/fl}$ controls at E18.5, respectively (Fig. 2A). Alizarin red and alcian blue-stained skeletal preparations of E18.5 *Adamts6*$^{del/del}$ embryos showed shortened hindlimbs with a clubfoot-like phenotype as compared to control (Fig. 2A). *Adamts6*$^{del/del}$ hindlimbs exhibit reduced length and gross morphological anomalies comparable to those observed in *Adamts6*$^{S149R/S149R}$ mutants, relative to their respective controls (Fig. 2B). Furthermore, the *Adamts6*$^{del/del}$ and *Adamts6*$^{S149R/S149R}$ femur, tibia, and fibula were shorter than those of *Adamts6*$^{fl/fl}$ and wild type mice, respectively (Fig. 2C). The axial skeleton of *Adamts6*$^{del/del}$ and *Adamts6*$^{S149R/S149R}$ mice exhibit malformed ribs, sternum, vertebral bodies and pelvic girdles (Supplementary Fig. 3). E14.5 *Adamts6*$^{del/del}$ limbs had reduced mineralization relative to wild type controls and showed that early limb development is defective (Supplementary Fig. 4A). Therefore, *Adamts6*$^{del/del}$ mice recapitulate the chondrodysplasia seen in *Adamts6*$^{S149R/S149R}$ mice, further demonstrating

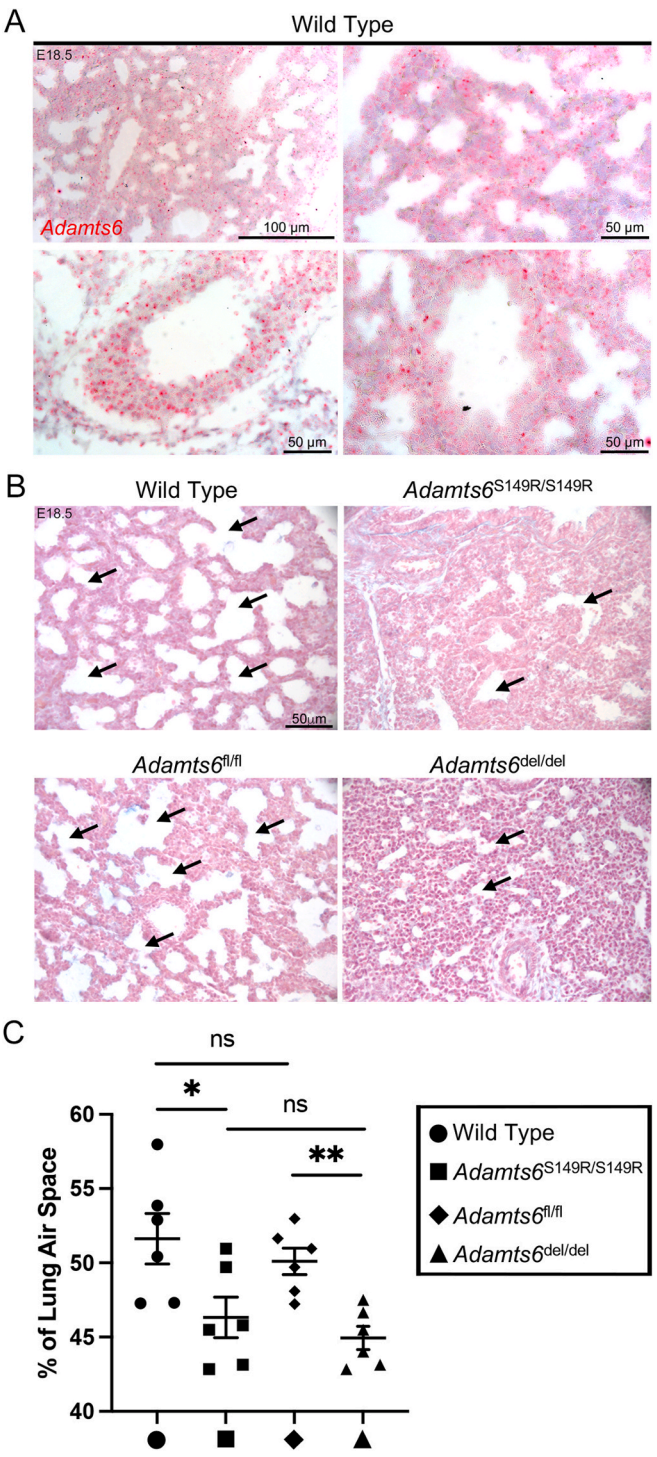

Fig. 4. *Adamts6*-deficient embryos exhibit delayed lung maturation. (A) RNAscope in situ hybridization demonstrated the presence of *Adamts6* transcripts in the lung parenchyma, airway walls, and blood vessel walls. **(B)** E18.5 lung sections revealed reduced pre-alveolar space in both *Adamts6*$^{S149R/S149R}$ and *Adamts6*$^{del/del}$ embryos compared to their respective wild type littermate controls. **(C)** Quantitative analysis of tissue density by airway space measurement from sections showed a significant reduction in *Adamts6*$^{S149R/S149R}$ and *Adamts6*$^{del/del}$ lungs relative to controls. n = 6. *p ≤ 0.05; **p ≤ 0.01.

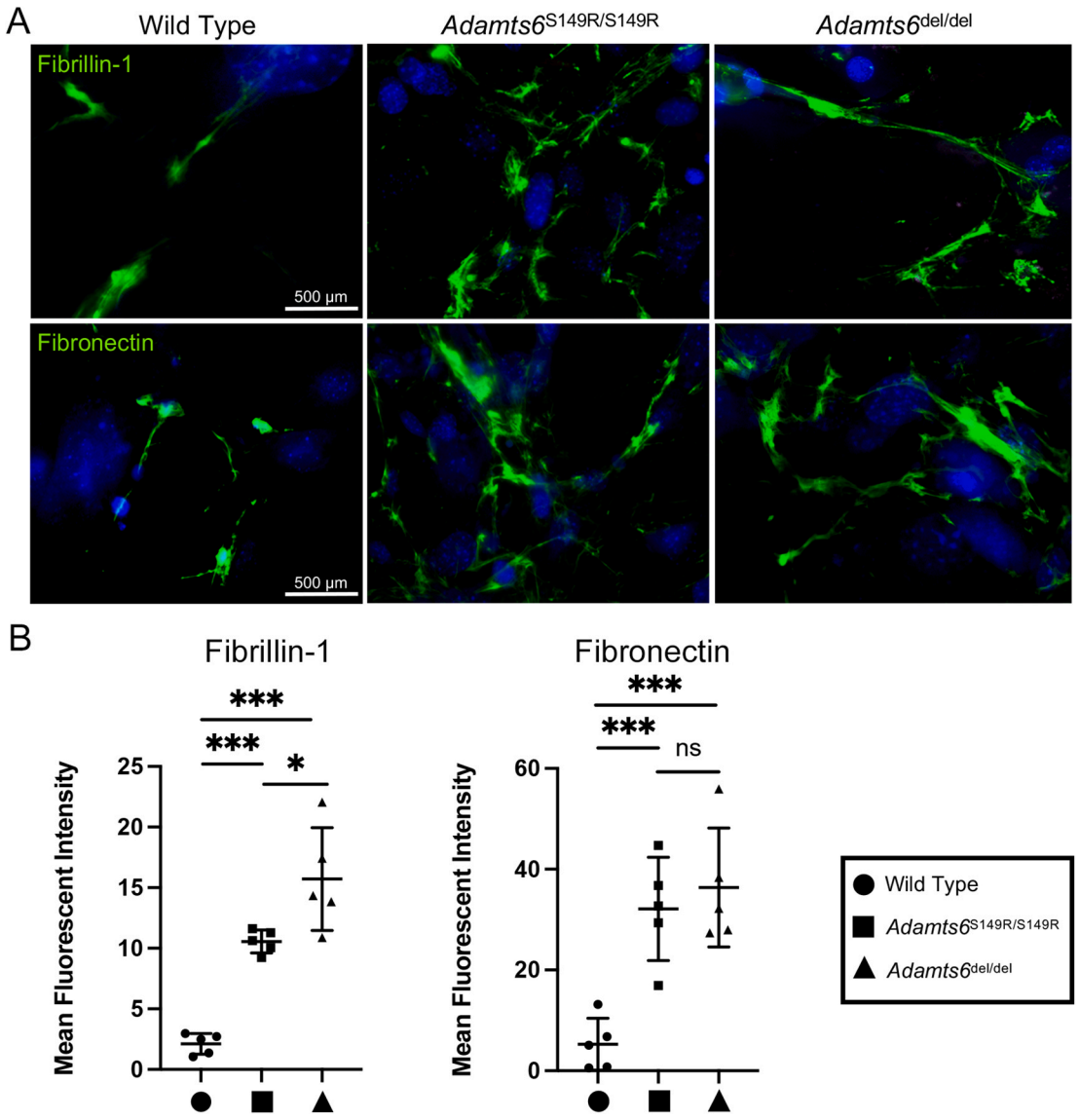

Fig. 5. Immunofluorescence staining of MEF cultures indicates increased staining of fibrillin-1 and fibronectin in *Adamts6*-deficient cultures. (A) *Adamts6*-deficient MEF cultures show an increase in fibrillin-1 and fibronectin staining when compared to wild type MEF cultures. **(B)** Quantification of fibrillin-1 and fibronectin in wild type, *Adamts6*$^{S149R/S149R}$ and *Adamts6*$^{del/del}$ MEF cultures showed significantly increased staining intensity of both ADAMTS6 targets. n = 12. *p ≤ 0.05; ***p ≤ 0.001.

correct gene targeting and efficiency of the *Adamts6*^{fl} allele.

Adamts6-deficient embryos have congenital heart defects

Adamts6 is widely expressed in the E18.5 developing heart. RNAscope in situ hybridization revealed *Adamts6* expression in the aortic valves (red box), the outflow tract (orange box), right ventricle (yellow box), interventricular septum (green box) and the left ventricle (blue box) (Fig. 3A). Alcian blue-staining of sections from E18.5 *Adamts6*$^{del/del}$ hearts identified a range of congenital heart defects analogous to those of *Adamts6*$^{S149R/S149R}$ embryos including ventricular septal defects (VSD), overriding aorta (OA) and double outlet right ventricle (DORV) (Fig. 3B). The prevalence of DORV and OA in *Adamts6*$^{del/del}$ embryos was similar to that of *Adamts6*$^{S149R/S149R}$ embryos. Specifically of the 51 *Adamts6*$^{S149R/S149R}$ mice, 33 % exhibited OA and 67 % had DORV whereas in 24 *Adamts6*$^{del/del}$ mice, 25 % had OA and 75 % had DORV. These congenital heart defects were apparent as early as E14.5 in *Adamts6*$^{del/del}$ hearts (Supplementary Fig. 4B).

Adamts6$^{del/del}$ *and Adamts6*$^{S149R/S149R}$ *embryos have underdeveloped lungs*

Widespread *Adamts6* expression was observed in the developing lung at E18.5, including developing pulmonary blood vessels, airway epithelium and alveolar saccules, as demonstrated by RNAscope in situ hybridization (Fig. 4A). Decreased pre-alveolar space in the *Adamts6*$^{del/del}$ and *Adamts6*$^{S149R/S149R}$ E18.5 lung sections was observed and is suggestive of pulmonary immaturity with arrest at the saccular stage (Fig. 4B and C). The underdevelopment of the lung is also apparent at E14.5, which demonstrates that ADAMTS6 is necessary for early lung formation and maturation (Supplementary Fig. 4C).

ECM of Adamts6$^{del/del}$ *MEFs has increased fibrillin-1 and fibronectin staining*

Fibrillin-1 and fibronectin, which are ADAMTS6 substrates, are components of the ECM necessary for connective tissue development [2]. *Adamts6*$^{del/del}$ and *Adamts6*$^{S149R/S149R}$ MEF cultures showed

increased staining for these proteins as compared to their respective controls (Fig. 5A). Quantification of the mean fluorescent signal intensity demonstrated a significant accumulation of fibrillin-1 in both *Adamts6*$^{S149R/S149R}$ and *Adamts6*$^{del/del}$ MEF cultures when compared to wild type controls (Fig. 5B). In addition to fibrillin-1, fibronectin staining intensity was also significantly elevated across *Adamts6*$^{S149R/S149R}$ and *Adamts6*$^{del/del}$ MEF cultures (Fig. 5B). Collectively, these results demonstrate that *Adamts6*$^{del/del}$ mice and their MEFs are a reliable model for investigating the consequences of ADAMTS6 deficiency.

Discussion

A floxed *Adamts6* mouse allele was generated using CRISPR-Cas9 and crossed with *CMV*-Cre and *Tagln*Cre for germline and cell-specific *Adamts6* inactivation, respectively. At the transcript level, to confirm successful deletion of *Adamts6* and validate the impact of our conditional knockout strategy, we performed RT-qPCR on cDNA from wild type and *Adamts6*$^{del/del}$ embryonic tissues and MEFs to show the deletion of exon 1, the targeted coding region in the floxed allele. Recapitulation of death at birth and skeletal and cardiac defects previously characterized in *Adamts6*$^{S149R/S149R}$ embryos confirmed correct gene targeting, which was necessary since antibodies useful for analysis of mouse ADAMTS6 protein are presently unavailable.

Since *Adamts6* is highly expressed in both normal and osteoarthritic cartilage and synovium, as identified through RT-qPCR analysis, and recently implicated in osteoarthritis in humans via multiomics, conditional deletion in specific musculoskeletal lineages, spatial domains and timelines could help dissect roles of ADAMTS6 in this condition [14,21,22]. The capability to selectively delete *Adamts6* in defined cardiac lineages provides a powerful tool to dissect its functional contribution to outflow tract remodeling and overall cardiac morphogenesis. Moreover, *Adamts6*$^{del/del}$ embryos have uncovered previously unrecognized pulmonary abnormalities, confirmed to also occur in the *Adamts6*$^{S149R/S149R}$ mutant. The histological demonstration of increased lung tissue density is suggestive of delayed lung maturation at the saccular stage, when the lungs have formed primitive alveoli preparatory to postnatally breathing [23]. This is a key transition phase for lung structure, surfactant production, and vascular development. During this stage of lung development, the ECM serves not only as a structural scaffold but also is essential for alveolar formation, via elastogenesis and ADAMTS6 may have a role regulating fibrillin microfibril and fibronectin turnover [24]. *Adamts6* may further influence pulmonary development by modulating the availability and activity of ECM-bound signaling molecules through these molecules, known to have a role in TGFβ and BMP activity, or other ECM substrates [25–27]. Fibrillin microfibrils also serve as a scaffold for elastic fiber assembly, which is important for alveolar development and passive recoil during respiration [28]. Loss of *Adamts6* is thus predicted to impair ECM remodeling, leading to dysregulated mechanical properties of lung tissue and impaired growth factor signaling, implying the need for further mechanistic investigation into its molecular and cellular functions through lineage and tissue-specific deletion.

Overall, the *Adamts6* floxed mouse serves as a valuable and versatile tool for studying ADAMTS6 function in a tissue-specific and temporal manner, providing critical insight into its role in skeletal, cardiac, and pulmonary development and likely other organs and tissues. Determining the role of ADAMTS6 is critical due to its essential involvement in ECM regulation, development, and adult tissue homeostasis. This model can address significant gaps in knowledge regarding the function of ADAMTS6 in adult physiology and its contribution to disease mechanisms.

CRediT authorship contribution statement

Jessica M. Sirek: Writing – review & editing, Writing – original draft, Visualization, Methodology, Investigation, Formal analysis, Data curation. **Elizabeth H. Rush:** Writing – review & editing, Methodology, Investigation, Formal analysis, Data curation. **Aditi Darodkar:** Writing – review & editing, Methodology, Investigation, Formal analysis, Data curation. **Suneel S. Apte:** Writing – review & editing, Resources, Funding acquisition. **Timothy J. Mead:** Writing – review & editing, Writing – original draft, Visualization, Validation, Supervision, Resources, Project administration, Methodology, Investigation, Funding acquisition, Formal analysis, Data curation, Conceptualization.

Declaration of competing interest

The authors declare that they have no known competing financial interests or personal relationships that could have appeared to influence the work reported in this paper.

Acknowledgments

This work was supported by funding from the National Institutes of Health (RO1HL15698701 to T.J.M.) and Paul G. Allen Frontiers Group (to S.S.A.). The authors would like to thank The Case Transgenic Core for their role in generation of the targeted allele and Connie Lin, Austin Hu, Deborah Seifert, Vinay Garg, and Gwyneth Li for technical assistance. We thank Dieter P. Reinhardt for the fibrillin-1 antibody.

Appendix A. Supplementary data

Supplementary data to this article can be found online at https://doi.org/10.1016/j.mbplus.2025.100186.

Data availability

Data will be made available on request.

References

[1] T.J. Mead, S.S. Apte, *ADAMTS proteins in human disorders*, Matrix Biology 71–72 (2018) 225–239.
[2] T.J. Mead, et al., *Proteolysis of fibrillin-2 microfibrils is essential for normal skeletal development*, eLife 11 (2022).
[3] J. Dubail, S.S. Apte, *Insights on ADAMTS proteases and ADAMTS-like proteins from mammalian genetics*, Matrix Biology 44–46 (2015) 24–37.
[4] B.P. Prins, et al., *Exome-chip meta-analysis identifies novel loci associated with cardiac conduction, including ADAMTS6*, Genome Biology 19 (1) (2018) 87.
[5] N. Dagoneau, et al., *ADAMTS10 mutations in autosomal recessive Weill-Marchesani syndrome*, The American Journal of Human Genetics 75 (5) (2004) 801–806.
[6] T.T. Luu, et al., *Overexpression of AGR2 is associated with drug resistance in mutant non-small cell lung cancers*, Anticancer Research 40 (4) (2020) 1855–1866.
[7] Y.P. Wang, Y.J. Zhao, X.L. Kong, *A metalloproteinase of the disintegrin and metalloproteinases and the ThromboSpondin Motifs 6 as a novel marker for colon cancer: functional experiments*, Genetics and Molecular Biology 43 (4) (2020).
[8] W.H. Xiao, et al., *Identification of commonly dysregulated genes in colorectal cancer by integrating analysis of RNA-Seq data and qRT-PCR validation*, Cancer Gene Therapy 22 (5) (2015) 278–284.
[9] Y. Xie, et al., *ADAMTS6 suppresses tumor progression via the ERK signaling pathway and serves as a prognostic marker in human breast cancer*, Oncotarget 7 (38) (2016) 61273–61283.
[10] X. Xu, et al., *Calcium channel TRPV6 promotes breast cancer metastasis by NFATC2IP*, Cancer Letters 519 (2021) 150–160.
[11] J. Huguet Herrero et al., *Loss of function variants in ADAMTS6 : Connective tissue, Heart defect, thoracic Aortic aneurysm and Neuro developmental Syndrome (CHANS)*. medRxiv, 2025.
[12] Y. Li, et al., *Global genetic analysis in mice unveils central role for cilia in congenital heart disease*, Nature 521 (7553) (2015) 520–524.
[13] S.A. Cain, et al., *ADAMTS-10 and -6 differentially regulate cell-cell junctions and focal adhesions*, Scientific Reports 6 (2016) 35956.
[14] K. Hatzikotoulas, et al., *Translational genomics of osteoarthritis in 1,962,069 individuals*, Nature 641 (8065) (2025) 1217–1224.
[15] Y.S. Tan, Y.L. Lei, *Generation and culture of mouse embryonic fibroblasts*, Methods in Molecular Biology 1960 (2019) 85–91.
[16] T.J. Mead, *Alizarin red and alcian blue preparations to visualize the skeleton*, Methods in Molecular Biology 2043 (2020) 207–212.
[17] A.B. Schroeder, et al., *The ImageJ ecosystem: open-source software for image visualization, processing, and analysis*, Protein Science 30 (1) (2021) 234–249.
[18] T.J. Mead, K.E. Yutzey, *Notch pathway regulation of chondrocyte differentiation and proliferation during appendicular and axial skeleton development*, Proceedings of the

National academy of Sciences of the United States of America 106 (34) (2009) 14420–14425.
[19] T.J. Mead, S.S. Apte, *Expression analysis by RNAscope in situ hybridization*, Methods in Molecular Biology 2043 (2020) 173–178.
[20] J. Schindelin, et al., *Fiji: an open-source platform for biological-image analysis*, Nature Methods 9 (7) (2012) 676–682.
[21] R.K. Davidson, et al., *Expression profiling of metalloproteinases and their inhibitors in synovium and cartilage*, Arthritis Research and Therapy 8 (4) (2006) R124.
[22] L. Kevorkian, et al., *Expression profiling of metalloproteinases and their inhibitors in cartilage*, Arthritis Rheum 50 (1) (2004) 131–141.
[23] J.C. Schittny, *Development of the lung*, Cell and Tissue Research 367 (3) (2017) 427–444.
[24] J.C. Valdoz, et al., *Soluble ECM promotes organotypic formation in lung alveolar model*, Biomaterials 283 (2022) 121464.
[25] S.L. Dallas, et al., *Dual role for the latent transforming growth factor-beta binding protein in storage of latent TGF-beta in the extracellular matrix and as a structural matrix protein*, The Journal of Cell Biology 131 (2) (1995) 539–549.
[26] F. Ramirez, D.B. Rifkin, *Extracellular microfibrils: contextual platforms for TGFbeta and BMP signaling*, Current Opinion in Cell Biology 21 (5) (2009) 616–622.
[27] H. Nistala, et al., *Fibrillin-1 and -2 differentially modulate endogenous TGF-beta and BMP bioavailability during bone formation*, The Journal of Cell Biology 190 (6) (2010) 1107–1121.
[28] A.R.F. Godwin, et al., *The role of fibrillin and microfibril binding proteins in elastin and elastic fibre assembly*, Matrix Biology 84 (2019) 17–30.